Higgs mode in a superfluid of Dirac fermions

Shunji Tsuchiya,[1] R. Ganesh,[2] and Tetsuro Nikuni[1]
[1]*Department of Physics, Faculty of Science, Tokyo University of Science, 1-3 Kagurazaka, Shinjuku-ku, Tokyo 162-8601, Japan*
[2]*Institute for Theoretical Solid State Physics, IFW Dresden, PF 270116, 01171 Dresden, Germany*
(Received 15 March 2013; published 26 July 2013)

We study the Higgs amplitude mode in the s-wave superfluid state on the honeycomb lattice inspired by recent cold atom experiments. We consider the attractive Hubbard model and focus on the vicinity of a quantum phase transition between semimetal and superfluid phases. On either side of the transition, we find collective mode excitations that are stable against decay into quasiparticle pairs. In the semimetal phase, the collective modes have "Cooperon" and exciton character. These modes smoothly evolve across the quantum phase transition, and become the Anderson-Bogoliubov mode and the Higgs mode of the superfluid phase. The collective modes are accommodated within a window in the quasiparticle-pair continuum, which arises as a consequence of the linear Dirac dispersion on the honeycomb lattice, and allows for sharp collective excitations. Bragg scattering can be used to measure these excitations in cold atom experiments, providing a rare example wherein collective modes can be tracked across a quantum phase transition.

DOI: 10.1103/PhysRevB.88.014527 PACS number(s): 03.75.Ss, 05.30.Rt, 71.10.Fd, 81.05.ue

I. INTRODUCTION

Spontaneous symmetry breaking of continuous symmetries gives rise to two typical collective excitations: gapless Goldstone modes and a gapped amplitude mode, also called the Higgs mode.[1] While the Goldstone mode has been observed in various contexts, the Higgs mode has evaded observation with rare exception such as $NbSe_2$ which has coexisting charge density wave and superconducting order,[2,3] "squashing" modes in ^{3}He,[4] and $Ba_2CoGe_2O_7$ with multiferroic order.[5] Remarkably, two recent experiments have successfully observed this mode by tracking collective excitations across a quantum phase transition. The first involves pressure studies of $TlCuCl_3$, a magnetic material which undergoes a transition from dimer order to magnetic order.[6] The second is the realization of the Bose-Hubbard model in ultracold gases, with a visible amplitude mode near the superfluid-Mott transition.[7–10]

In this paper, we propose a scheme to observe a *pure* Higgs amplitude mode in a *Fermi* superfluid. The Higgs mode has previously been observed in fermionic ^{3}He,[4] but due to the triplet p-wave nature of pairing, it occurs mixed with angular momentum character. Our proposal is more transparent involving a pure amplitude mode in a simple s-wave superfluid. Hitherto, such a mode has never been seen as it typically decays into pairs of quasiparticles.[1] Our proposal circumvents this issue by exploiting a special feature of the honeycomb lattice geometry which allows for a window in the quasiparticle-pair continuum; the Higgs mode can survive as a stable excitation inside this window.

Inspired by the recent realization of the honeycomb optical lattices in cold atom experiments,[11] we study the attractive Hubbard model in this geometry:

$$H = -\sum_{i,j,\sigma} t_{ij} c^{\dagger}_{i\sigma} c_{j\sigma} - \mu \sum_{i,\sigma} n_{i\sigma} - U \sum_{i} n_{i\uparrow} n_{i\downarrow}. \qquad (1)$$

Parameter t_{ij} denotes hopping amplitude between nearest-neighbor ($t_{ij} = t$) and next-nearest-neighbor sites ($t_{ij} = t'$). U is an onsite attractive interaction and μ is the chemical potential. We envisage a setup with a deep optical lattice to trap two hyperfine species of fermions, and a magnetic field on the attractive side of a Feshbach resonance.[12] This model hosts a superfluid state of Dirac fermions, with several interesting implications.[13,14] In this proposal, we make use of two key features: (i) strictly at half-filling, there is an interaction-tuned quantum phase transition from a semimetal phase to an s-wave superfluid. This has been demonstrated by sophisticated quantum Monte Carlo simulations on very large system sizes.[15,16] Reference 17 has reinforced the continuous nature of this transition by demonstrating good data collapse with critical exponents in the Gross-Neveu universality class. This transition is a consequence of the Dirac cone dispersion which leads to vanishing density of states at the Fermi level, thereby necessitating a critical interaction strength to induce superfluid order.[13,18] (ii) In the semimetal phase, the two-particle continuum has a window structure, again a consequence of the Dirac cone dispersion.[19] A collective mode excitation propagating inside this window is stable against decay into quasiparticle pairs. We show that this window structure persists in the superfluid phase, thus allowing for a stable Higgs mode excitation.

The phase diagram of this model at half-filling is shown in Fig. 1(b). Our two key findings are summarized in Figs. 1(c)–1(f): (i) on either side of the transition, there are collective mode excitations which are stable against decay into quasiparticle pairs. The two-particle continuum is shown as the shaded region: note the window structure. In the semimetal phase, there are three degenerate collective modes with "Cooperon" and exciton character. On the superfluid side, there is a Goldstone mode and, remarkably, a distinct superfluid amplitude (Higgs) mode. (ii) Cooperons and exciton excitations in the semimetal phase smoothly evolve into the Goldstone mode and the Higgs mode in the superfluid phase across the quantum critical point.

Even though our calculations ignore damping from processes beyond the random phase approximation (RPA) level, we believe these collective modes to be well defined and observable. Indeed, they can be observed in a cold atom experiment using Bragg scattering, a rare example wherein relevant collective excitations can be tracked on both sides

of a quantum phase transition. We discuss the stability and observability of these modes in greater detail in Sec. VII.

II. MEAN FIELD THEORY

The Swiss Federation of Technology (ETH) group[11] has studied fermions loaded onto a honeycomb optical lattice with tunable anisotropy. We consider the attractive Hubbard model in the *isotropic* honeycomb lattice. As discussed in Ref. 14, the isotropic limit is expected to have the highest superfluid transition temperature and is the most promising for experimental realization. We decompose the Hubbard interaction in the superfluid channel using the order parameter $\Delta = U\langle c_{i\downarrow}c_{i\uparrow}\rangle$, taken to be real. For brevity, we introduce a vector operator consisting of creation and annihilation operators $\hat{\Psi}(\boldsymbol{p}) = (c_{\boldsymbol{p},a,\uparrow}, c^{\dagger}_{-\boldsymbol{p},a,\downarrow}, c_{\boldsymbol{p},b,\uparrow}, c^{\dagger}_{-\boldsymbol{p},b,\downarrow})^t$ [a and b denote the two sublattices as shown in Fig. 1(a)]. The mean field Hamiltonian can be written as

$$H_{\mathrm{MF}} = \sum_{\boldsymbol{p}} \hat{\Psi}^{\dagger}(\boldsymbol{p})\hat{h}(\boldsymbol{p})\hat{\Psi}(\boldsymbol{p}), \tag{2}$$

where $\hat{h}(\boldsymbol{p}) = \{x_{\boldsymbol{p}} + \mathrm{Re}(\gamma_{\boldsymbol{p}})\sigma_x - \mathrm{Im}(\gamma_{\boldsymbol{p}})\sigma_y\}\tau_3 - \Delta\tau_1$, $\gamma_{\boldsymbol{p}} = -t(1 + e^{i\boldsymbol{p}\cdot\boldsymbol{a}_1} + e^{i\boldsymbol{p}\cdot\boldsymbol{a}_2})$, and $x_{\boldsymbol{p}} = -2t'\{\cos(\boldsymbol{p}\cdot\boldsymbol{a}_1) + \cos(\boldsymbol{p}\cdot\boldsymbol{a}_2) + \cos[\boldsymbol{p}\cdot(\boldsymbol{a}_1 - \boldsymbol{a}_2)]\} - \mu$ with $\boldsymbol{a}_1$ and $\boldsymbol{a}_2$ being the two basis vectors shown in Fig. 1(a). We take the lattice spacing to be unity. $\vec{\tau}$ and $\vec{\sigma}$ are the Pauli matrices in the Nambu and sublattice spaces, respectively. The single-particle Green's function for the mean field Hamiltonian is given by

$$\hat{G}(p) = \left[i\omega_n - \hat{h}(\boldsymbol{p})\right]^{-1} \equiv \begin{pmatrix} \hat{G}^{aa}(p) & \hat{G}^{ab}(p) \\ \hat{G}^{ba}(p) & \hat{G}^{bb}(p) \end{pmatrix}. \tag{3}$$

Here, we denote $p = (\boldsymbol{p}, i\omega_n)$, where ω_n is the fermion Matsubara frequency. The gap and number equations are obtained from the off-diagonal and diagonal elements of the Green's function $\hat{G}^{\nu\nu}$ as[13] (hereafter, we restrict ourselves to zero temperature)

$$\frac{1}{U} = \frac{1}{N}\sum_{\boldsymbol{p}}\sum_{\alpha=\pm}\frac{1}{2E^{\alpha}(\boldsymbol{p})}, \tag{4}$$

$$n = 1 - \frac{1}{N}\sum_{\boldsymbol{p}}\sum_{\alpha=\pm}\frac{\xi^{\alpha}_{\boldsymbol{p}}}{E^{\alpha}(\boldsymbol{p})}, \tag{5}$$

where $E^{\pm}(\boldsymbol{p}) = \sqrt{(\xi^{\pm}_{\boldsymbol{p}})^2 + \Delta^2}$ is the spectrum of the Bogoliubov quasiparticles, $\xi^{\pm}_{\boldsymbol{p}} = x_{\boldsymbol{p}} \pm |\gamma_{\boldsymbol{p}}|$, and N is the number of lattice sites. At half-filling, the self-consistent solution of Δ becomes nonzero for $U > U_c$, indicating a transition from semimetal to superfluid phases.[13,14] For $t' = 0$, mean-field theory gives $U_c \sim 2.23t$. Quantum Monte Carlo gives the same transition, except with U_c renormalized to $\sim$3.869.[15] In the rest of this paper, we use mean field results with the understanding that fluctuations will renormalize U quantitatively. We note that U_c weakly depends on the value of t'.

III. GENERALIZED RANDOM PHASE APPROXIMATION (GRPA)

On either side of the critical point, there are low-lying density and pairing fluctuations. We use a generalized random phase approximation (GRPA) scheme to evaluate density and pairing response functions. We follow the Green's function approach of Côté and Griffin,[20] which evaluates susceptibilities by summing over ladder diagrams and bubble diagrams. We denote matrix susceptibilities containing the response to weak density and pairing perturbations, respectively, as

$$\hat{L}^{\nu_1\nu_2}(q) = \begin{pmatrix} \chi^{\nu_1\nu_2}_{n_\uparrow n}(q) & \chi^{\nu_1\nu_2}_{mn}(q) \\ -\chi^{\nu_1\nu_2}_{m^\dagger n}(q) & \chi^{\nu_1\nu_2}_{n_\downarrow n}(q) \end{pmatrix}, \tag{6}$$

$$\hat{M}^{\nu_1\nu_2}(q) = \begin{pmatrix} \chi^{\nu_1\nu_2}_{n_\uparrow m^\dagger}(q) & \chi^{\nu_1\nu_2}_{mm^\dagger}(q) \\ -\chi^{\nu_1\nu_2}_{m^\dagger m^\dagger}(q) & \chi^{\nu_1\nu_2}_{n_\downarrow m^\dagger}(q) \end{pmatrix}, \tag{7}$$

where $q = (\boldsymbol{q}, i\Omega_n)$ (Ω_n is a boson Matsubara frequency). Any susceptibility χ is defined as

$$\chi^{\nu_1\nu_2}_{fg}(q) = -\sum_{\boldsymbol{r}_{12}}\int_0^{\beta} d\tau_{12}\langle T_\tau \delta f(1)\delta g(2)\rangle e^{-i(\boldsymbol{q}\cdot\boldsymbol{r}_{12} - \Omega_n\tau_{12})}, \tag{8}$$

where $1 \equiv (\boldsymbol{r}_{l_1}, \nu_1, \tau_1)$ (l_1 denotes the unit cell, ν_1 the sublattice, and τ_1 an imaginary time), $\boldsymbol{r}_{12} = \boldsymbol{r}_{l_1} - \boldsymbol{r}_{l_2}$, $\tau_{12} = \tau_1 - \tau_2$, and $\delta f \equiv f - \langle f\rangle$. The density and pair annihilation operators are written as $n = n_\uparrow + n_\downarrow$ and $m = c_\downarrow c_\uparrow$, respectively. The GRPA equations read as[14,20]

$$\bar{A}^{\nu_1\nu_2}(q) = \hat{A}^{0\nu_1\nu_2}(q) + \frac{2U}{\beta N}\sum_{\nu_3}\sum_{\boldsymbol{p},\omega_n}\tilde{G}^{\nu_1\nu_3}(p+q) \times \bar{A}^{\nu_3\nu_2}(q)\tilde{G}^{\nu_3\nu_1}(p), \tag{9}$$

$$\hat{A}^{\nu_1\nu_2}(q) = \bar{A}^{\nu_1\nu_2}(q) - U\sum_{\nu_3}\bar{L}^{\nu_1\nu_3}(q)\mathrm{Tr}\{\hat{A}^{\nu_3\nu_2}(q)\}, \tag{10}$$

where A is either L or M and $\tilde{G}^{\nu_1\nu_2}(p) = \tau_3\hat{G}^{\nu_1\nu_2}(p)$. A^0 denotes the bare susceptibility,[21] $\bar{A}$ includes an infinite sum over ladder diagrams, while $\hat{A}$ is the final result which also includes bubble diagrams.

IV. HIGGS MODE IN THE SUPERFLUID

In the superfluid phase, we solve GRPA equations (9) and (10) to evaluate the amplitude and phase correlation functions $\chi^{\nu_1\nu_2}_{\Delta\Delta}(q) = \frac{U^2}{2}[\chi^{\nu_1\nu_2}_{mm^\dagger}(q) + \chi^{\nu_1\nu_2}_{m^\dagger m}(q)]$ and $\chi^{\nu_1\nu_2}_{\theta\theta}(q) = \frac{U^2}{2\Delta^2}[\chi^{\nu_1\nu_2}_{mm^\dagger}(q) - \chi^{\nu_1\nu_2}_{m^\dagger m}(q)]$. The amplitude and phase fluctuation operators are given by $\delta\Delta = \frac{U}{2}(\delta m + \delta m^\dagger)$ and $\delta\theta = \frac{U}{2i\Delta}(\delta m - \delta m^\dagger)$, respectively. For the case of $t' = 0$, the expressions simplify and we can identify their respective poles, which we denote "Higgs" and "AB/Leggett." These poles satisfy

$$\text{Higgs}: \quad \frac{1}{U} = -(C + D) + |R|, \tag{11}$$

$$\text{AB/Leggett}: \quad \frac{1}{U} = -(C - D) + \sqrt{4F^2 + |R|^2}. \tag{12}$$

We have defined

$$C = \frac{1}{N}\sum_{\boldsymbol{p}}\frac{E + E'}{(i\Omega_n)^2 - (E + E')^2}, \tag{13}$$

$$D = -\frac{1}{N}\sum_{\boldsymbol{p}}\frac{\Delta^2}{E'E}\frac{E + E'}{(i\Omega_n)^2 - (E + E')^2}, \tag{14}$$

$$F = \frac{1}{N}\sum_{\boldsymbol{p}} \frac{\Delta}{E}\frac{i\Omega_n}{(i\Omega_n)^2-(E+E')^2}, \tag{15}$$

$$R = -\frac{1}{N}\sum_{\boldsymbol{p}} \frac{\gamma'\gamma^*}{E'E}\frac{E+E'}{(i\Omega_n)^2-(E+E')^2}. \tag{16}$$

Here, we have denoted $E = E(\boldsymbol{p})$, $E' = E(\boldsymbol{p}+\boldsymbol{q})$, $\gamma = \gamma_{\boldsymbol{p}}$, and $\gamma' = \gamma_{\boldsymbol{p}+\boldsymbol{q}}$. On the other hand, solving Eqs. (9) and (10) for density response, we find that $\chi_{\theta\theta}^{\nu_1\nu_2}(q) \propto \chi_{nn}^{\nu_1\nu_2}(q)$ when $t' = 0$. Thus, the density response function only retains the AB/Leggett pole given in Eq. (12).

Setting $\boldsymbol{q} = \Omega_n = 0$ in Eq. (12), we recover the gap equation (4). Thus, the superfluid phase has *gapless* collective mode(s) arising from phase fluctuations. In fact, at half-filling, the AB/Leggett pole in Eq. (12) is a double pole corresponding to two gapless modes: the Anderson-Bogoliubov (AB) mode and the Leggett mode.[14] The AB mode is the usual Goldstone mode associated with U(1) symmetry breaking.[22,23] The Leggett mode is composed of out-of-phase fluctuations between sublattices[24]: it acquires a gap away from half-filling.[14] The AB and Leggett modes become degenerate at half-filling, reflecting a special pseudospin SU(2) symmetry of the Hubbard model.[14] For small $q \ll 1$, Eq. (12) gives the dispersion relation of the AB/Leggett mode to be[25]

$$\omega_{\rm AB} = \lambda v_F q, \;\; \lambda^2 = \frac{U}{N}\sum_{\boldsymbol{p}} \frac{|\gamma|^2}{E^3} \leqslant 1, \tag{17}$$

where $v_F = 3t/2$ is the Fermi velocity at the Dirac points. Thus, the AB mode propagates at speeds smaller than v_F.

Setting $(\boldsymbol{q}, i\Omega_n) = (0, 2\Delta)$, Eq. (11) also reduces to the gap equation. Thus, there exists a *gapped* collective mode with the energy gap 2Δ at $\boldsymbol{q} = 0$. This is the Higgs mode or the amplitude mode[3] arising from amplitude fluctuations of the superfluid order parameter. It can be understood using the mechanical analog of motion along the radial direction of the famous "Mexican hat" potential; the energy gap stems from the finite curvature of the potential along the radial direction. The gap of the Higgs mode is twice as large as that of quasiparticle excitations. This result agrees with Ref. 3 where it is understood as arising from the invariance of the Hamiltonian under a certain local nonunitary transformation of the field operator and the resulting continuity equation for Cooper pair density.[3,26]

Remarkably, the Higgs mode disperses below the quasiparticle pair continuum in Figs. 1(e) and 1(f). In particular, close to the M point, it is well separated from the lower edge of the continuum. This is to be contrasted with the case of typical superfluids: due to the underlying Fermi surface, the continuum exhibits a horizontal edge near $q \sim 0$.[3] The Higgs mode therefore enters the continuum, becomes heavily damped, and is unobservable.

In our case, the Higgs mode in Fig. 1 is undamped over large sections of the Brillouin zone. This window or arch in the continuum, shown in Fig. 1, is a consequence of the Dirac-type dispersion of underlying fermions. The Higgs mode stays undamped as long as it lies within this window. For $q \ll 1$, solving Eq. (11), the Higgs mode has the dispersion relation $\omega_{\rm Higgs}^2 = 4\Delta^2 + v_F^2 q^2$.[25] The lower edge of the continuum, which is given by $\omega_{\rm edge}^2 = \min_{\boldsymbol{p}}\{[E(\boldsymbol{p}) + E(\boldsymbol{p}+\boldsymbol{q})]^2\}$, has

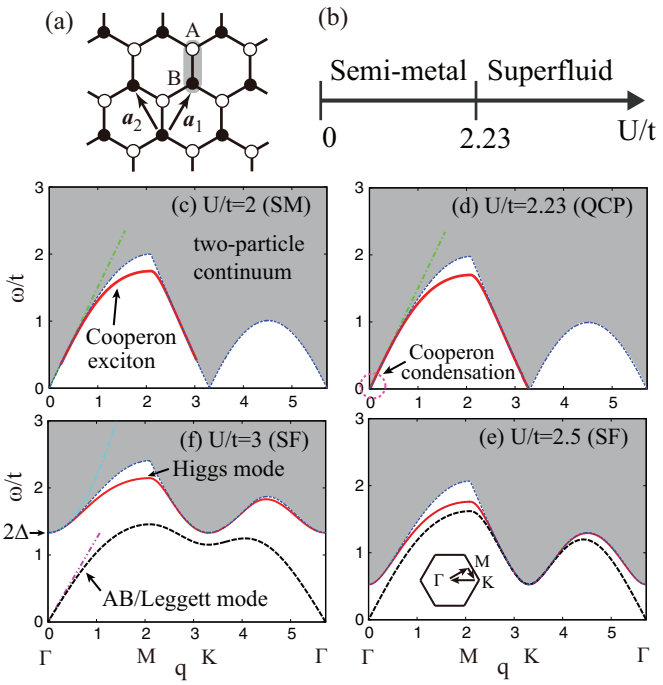

FIG. 1. (Color online) Isotropic honeycomb lattice with basis vectors (a). Phase diagram of the attractive Hubbard model on a honeycomb lattice at half-filling with $t' = 0$ as obtained from the mean field theory (b). Evolution of the elementary excitations across the quantum critical point (QCP) of the semimetal (SM) to superfluid (SF) phase transition (c)–(f). The dashed-dotted line in each panel shows the asymptotic dispersion ($q \ll 1$) of the continuum edge which overlaps with the Higgs mode in (f). The dashed-dotted-dotted line in (f) shows the asymptotic dispersion of the AB/Leggett mode.

the same asymptotic form $\omega_{\rm edge}^2 \simeq 4\Delta^2 + v_F^2 q^2$ ($q \ll 1$). The deviation of the Higgs mode from the lower edge of the continuum starts from higher order in q, which is beyond the Dirac-type linear dispersion. Even if we go slightly away from half-filling, the Higgs mode survives undamped. Close to $n \sim 0.9$ or 1.1, the window disappears because of the presence of the Fermi surface; as a result, the Higgs mode is strongly damped. The Higgs mode, the AB mode, and the lower edge of the continuum become degenerate at the QCP for $q \ll 1$: $\omega_{\rm AB} = \omega_{\rm Higgs} = \omega_{\rm edge} = v_F q$.

The AB and Leggett modes are strongly coupled with density fluctuations; they appear as poles in the density response function $\chi_{nn}^{\nu_1\nu_2}(q)$. However, when $t' = 0$, the Higgs mode has no corresponding pole in the density response function. Thus, the Higgs mode is composed of pure amplitude fluctuations and can not be excited by a density perturbation. This reflects the underlying SU(2) pseudospin symmetry[14] in the problem. A small finite t' breaks this symmetry and forces the Higgs mode to acquire a density component: the density response then shows a peak at the Higgs mode, as shown in Fig. 2.

V. COOPERONS AND EXCITONS IN THE SEMIMETAL

In the semimetal phase, setting $\Delta = 0$, density and pair response functions become decoupled in the GRPA equations (9) and (10). The susceptibilities satisfy the usual RPA equations

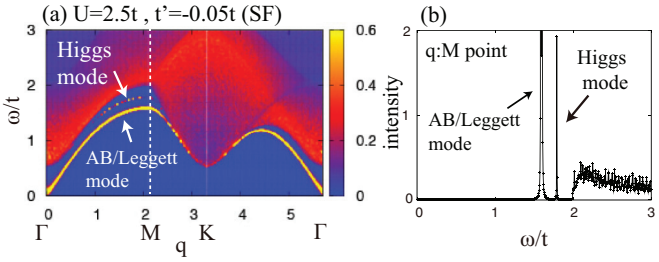

FIG. 2. (Color online) Intensity of dynamic structure factor corresponding to density response $S(\boldsymbol{q},\omega) = -\mathrm{Im}[\chi_{nn}(\boldsymbol{q},\omega)]/\pi$ for $t' = -0.05t$ (a). The cross section for the momentum at the M point (b). The upper peak corresponds to the Higgs mode.

$\chi^{\nu_1\nu_2}_{mm^\dagger}(q) = \chi^{0\nu_1\nu_2}_{mm^\dagger}(q) + U\sum_{\nu_3}\chi^{0\nu_1\nu_3}_{mm^\dagger}(q)\chi^{\nu_3\nu_2}_{mm^\dagger}(q)$, $\chi^{\nu_1\nu_2}_{n_\sigma n}(q) = \chi^{0\nu_1\nu_2}_{n_\sigma n}(q) - U\sum_{\nu_3}\chi^{0\nu_1\nu_3}_{n_\sigma n}(q)\chi^{\nu_3\nu_2}_{n_{-\sigma} n}(q)$. The bare susceptibility $\chi^0_{mm^\dagger}$ describes a single rung diagram with particle-particle (hole-hole) excitations, and $\chi^0_{n_\sigma n}$ describes a single bubble diagram with particle-hole excitations. They are given by

$$\chi^{0\nu_1\nu_2}_{mm^\dagger}(q) = \frac{1}{2N}\sum_{\boldsymbol{p}}\left[\frac{\kappa^{\nu_1\nu_2}_{\boldsymbol{p}}\kappa^{\nu_1\nu_2}_{\boldsymbol{q}-\boldsymbol{p}}}{\xi^+_{\boldsymbol{p}}+\xi^+_{\boldsymbol{q}-\boldsymbol{p}}-i\Omega_n} - \frac{\eta^{\nu_1\nu_2}_{\boldsymbol{p}}\eta^{\nu_1\nu_2}_{\boldsymbol{q}-\boldsymbol{p}}}{\xi^-_{\boldsymbol{p}}+\xi^-_{\boldsymbol{q}-\boldsymbol{p}}-i\Omega_n}\right], \quad (18)$$

$$\chi^{0\nu_1\nu_2}_{n_\sigma n}(q) = \frac{1}{2N}\sum_{\boldsymbol{p}}\left[\frac{-\kappa^{\nu_1\nu_2}_{\boldsymbol{p}+\boldsymbol{q}}\eta^{\nu_2\nu_1}_{\boldsymbol{p}}}{\xi^+_{\boldsymbol{p}+\boldsymbol{q}}-\xi^-_{\boldsymbol{p}}-i\Omega_n} + \frac{\eta^{\nu_1\nu_2}_{\boldsymbol{p}+\boldsymbol{q}}\kappa^{\nu_2\nu_1}_{\boldsymbol{p}}}{\xi^-_{\boldsymbol{p}+\boldsymbol{q}}-\xi^+_{\boldsymbol{p}}-i\Omega_n}\right], \quad (19)$$

where $\kappa^{\nu_1\nu_2}_{\boldsymbol{p}} = \delta_{\nu_1\nu_2} + e^{i\phi_{\boldsymbol{p}}}\delta_{\nu_1 a}\delta_{\nu_2 b} + e^{-i\phi_{\boldsymbol{p}}}\delta_{\nu_1 b}\delta_{\nu_2 a}$ and $\eta^{\nu_1\nu_2}_{\boldsymbol{p}} = \delta_{\nu_1\nu_2} - e^{i\phi_{\boldsymbol{p}}}\delta_{\nu_1 a}\delta_{\nu_2 b} - e^{-i\phi_{\boldsymbol{p}}}\delta_{\nu_1 b}\delta_{\nu_2 a}$. We denote $e^{i\phi_{\boldsymbol{p}}} = \gamma_{\boldsymbol{p}}/|\gamma_{\boldsymbol{p}}|$.

From the denominator in Eq. (18), we see that pairing response arises from particle-particle (or hole-hole) excitations. An undamped pairing mode, occurring below the particle-particle continuum in Fig. 1(c), is therefore a two-particle bound state with well-defined momentum and energy. It can be understood as a preformed Cooper pair: we call this a *Cooperon* excitation.[27] Similarly, from Eq. (19), we see that density response arises from particle-hole excitations. An undamped density mode is thus a particle-hole bound state: we call this an *exciton*.

The dispersions of Cooperons and excitons are determined by the poles of the corresponding response functions, giving $|\hat{I} - U\hat{\chi}_{mm^\dagger}(q)| = 0$ and $|\hat{I} + U\hat{\chi}^0_{n_\sigma n}(q)| = 0$. With $t' = 0$, these reduce to the identical equation

$$[1 + U\alpha(q)]^2 - U^2|\beta(q)|^2 = 0, \quad (20)$$

$$\alpha(q) = \frac{1}{N}\sum_{\boldsymbol{p}}\frac{|\gamma_{\boldsymbol{p}}| + |\gamma_{\boldsymbol{p}+\boldsymbol{q}}|}{(i\Omega_n)^2 - (|\gamma_{\boldsymbol{p}}| + |\gamma_{\boldsymbol{p}+\boldsymbol{q}}|)}, \quad (21)$$

$$\beta(q) = -\frac{1}{N}\sum_{\boldsymbol{p}}\frac{e^{i(\phi_{\boldsymbol{p}+\boldsymbol{q}}-\phi_{\boldsymbol{p}})}(|\gamma_{\boldsymbol{p}}| + |\gamma_{\boldsymbol{p}+\boldsymbol{q}}|)}{(i\Omega_n)^2 - (|\gamma_{\boldsymbol{p}}| + |\gamma_{\boldsymbol{p}+\boldsymbol{q}}|)^2}. \quad (22)$$

Thus, the Cooperon and the exciton are degenerate when $t' = 0$. Their dispersion is shown in Figs. 1(c) and 1(d); the modes are undamped at the RPA level as they lie below the two-particle continuum. In particular, they are well separated from the continuum in the vicinity of the M points. We suggest that experiments should probe this region to observe the collective excitations. This feature of the M points can be understood from the single-particle band structure which has saddle points at these wave vectors. They consequently have a very large density of states which provides large phase space for the Hubbard interaction to form two-particle bound states.

These collective modes in the semimetal phase were predicted many years ago, using an insightful single-cone approximation: Ref. 19 reported a triplet exciton mode in the repulsive Hubbard model. The authors identified the window structure in the continuum as capable of accommodating stable modes. Mapping their results to the attractive Hubbard case,[16] the triplet excitons translate to Cooperon and exciton modes. We reaffirm their prediction, starting from a microscopic picture taking into account the sublattice structure. Our expressions also agree with those of Ref. 28, which only considers the $\Gamma - K$ segment and concludes that there is no undamped mode. However, we find an undamped mode in the $\Gamma - M$ and $M - K$ directions.

VI. COOPERON CONDENSATION

As we approach the critical point from the semimetal side, the energy of the Cooperon and exciton decreases progressively [see Figs. 1(c) and 1(d)]. Precisely at the transition, the Cooperon "softens" at $\boldsymbol{q} = 0$ and undergoes condensation. In fact, setting $\boldsymbol{q} = \Omega_n = 0$, the Cooperon pole in Eq. (20) reduces to the gap equation (4). Our results present an elegant picture in which the quantum phase transition from semimetal to superfluid can be understood as Cooperon condensation. Since Cooperons and excitons are degenerate for $t' = 0$, the exciton can also condense at the critical point. That gives rise to the sublattice charge density wave (CDW) state, which is degenerate with the superfluid state due to SU(2) pseudospin symmetry. For $t' \neq 0$, this degeneracy is lifted in favor of the superfluid and the Cooperon condenses preferentially.

As we cross U_c and enter the superfluid phase, Cooperons and excitons hybridize to become the AB, Leggett, and Higgs modes. The excitonic component, when present, allows these modes to have peaks in the density response function. The cooperonic component manifests as peaks in the pairing response. Thus, the collective modes evolve smoothly across the QCP and carry signatures of the underlying spontaneous symmetry breaking.

VII. VISIBILITY OF COLLECTIVE MODES

In both the semimetal and superfluid phases, we find stable collective excitations within GRPA. We have demonstrated that in the vicinity of the M points, these modes do not decay into pairs of quasiparticles. However, there can be damping processes beyond the GRPA which lie beyond the scope of this paper, for example, the Higgs mode may decay into two AB modes. While a more involved calculation is required, the GRPA results are a strong indication that we may find well-defined collective modes. In the limit $U \gg U_c$, we expect our AB and Leggett modes to map onto spin-wave results.[14] As the ground state is collinear, we expect the spin waves to be undamped.[29] For $U < U_c$, in the semimetal phase,

we have Cooperons and excitons in the vicinity of the M points. These states are akin to excitons occurring at the Brillouin zone edge which are known from semiconductor physics.[30] With this analogy, we expect the modes to be stable for $U < U_c$.

We can not comment on the stability of these modes in the critical region in which magnitude of order parameter is comparable with amplitude fluctuation. But, we expect to see undamped modes on either side of the transition away from the critical region. We suggest Bragg spectroscopy measurements on a Fermi superfluid in a honeycomb optical lattice as a way to measure these modes. In this technique, a two-photon process imparts a density- "kick" to the system. The response to this perturbation can be quantified by measuring the momentum transferred or the energy absorbed. The momentum transferred is a measure of the dynamic structure factor related to the density response function $S(\boldsymbol{q},\omega) = -\mathrm{Im}[\chi_{nn}(\boldsymbol{q},\omega)]/\pi$ (Ref. 31): it can detect collective modes as long as they have a density component.

The observability of the Higgs mode itself is an interesting question. Our Higgs mode is stable against decay into pairs of fermions due to the window structure in the two-particle continuum. A recent proposal finds a similar Higgs mode in the d-wave superconductors.[32] In our semimetal-to-superfluid transition, due to the pseudospin symmetry present when $t' = 0$, the order parameter can be thought of as an O(3) object. Quantum Monte Carlo simulations of the O(3) ordering transition show that the Higgs mode survives in the "scalar" susceptibility, although it is broadened by decay into Goldstone bosons.[33] We note that our suggestion is to look for the Higgs mode at the M points far away from Γ, the wave vector at which Cooperon condensation takes place. To our knowledge, there has been no calculation of the damping of the amplitude mode away from the Γ point. Bragg scattering measurements could well be able to identify a well-defined Higgs mode. To be visible with Bragg spectroscopy, the Higgs mode should have a density component which can arise from a nonzero t' hopping. We expect any real optical lattice configuration to have a small nonzero t'.[34] This term breaks the pseudospin SU(2) symmetry of the Hamiltonian, and adds a small density component to the Higgs mode. Figure 2 shows $S(\boldsymbol{q},\omega)$ for $t' = -0.05$. The sharp intensity peak for the Higgs mode can be clearly seen below the continuum. An alternative approach is to measure the energy absorption in response to a weak shaking of the optical lattice.[9]

ACKNOWLEDGMENTS

We acknowledge A. Paramekanti for fruitful dicussions. S.T. thanks M. Sigrist, T. Esslinger, L. Tarruell, Y. Ohashi, S. Okada, S. Konabe, K. Asano, S. Kurihara, and K. Kamide for discussions. S.T. was supported by Grant-in-Aid for Scientific Research, Grant No. 24740276.

APPENDIX A: BARE SUSCEPTIBILITY IN GRPA

To solve the GRPA equations (8) and (9), the bare susceptibilities L^0 and M^0 are evaluated using the mean field Green's function in Eq. (2) to give

$$\hat{L}^{0\nu_1\nu_2}(q) = \frac{1}{\beta M}\sum_{\boldsymbol{p},\omega_n}\tilde{G}^{\nu_1\nu_2}(p+q)\tilde{G}^{\nu_2\nu_1}(p) = \begin{pmatrix} L^{0\nu_1\nu_2}_{1111}+L^{0\nu_1\nu_2}_{1221} & L^{0\nu_1\nu_2}_{1112}+L^{0\nu_1\nu_2}_{1222} \\ L^{0\nu_1\nu_2}_{2111}+L^{0\nu_1\nu_2}_{2221} & L^{0\nu_1\nu_2}_{2112}+L^{0\nu_1\nu_2}_{2222}\end{pmatrix}, \tag{A1}$$

$$\hat{M}^{0\nu_1\nu_2}(q) = \frac{1}{\beta M}\sum_{\boldsymbol{p},\omega_n}\tilde{G}^{\nu_1\nu_2}(p+q)\begin{pmatrix}0&1\\0&0\end{pmatrix}\tilde{G}^{\nu_2\nu_1}(p) = \begin{pmatrix} L^{0\nu_1\nu_2}_{1121} & L^{0\nu_1\nu_2}_{1122} \\ L^{0\nu_1\nu_2}_{2121} & L^{0\nu_1\nu_2}_{2122}\end{pmatrix}, \tag{A2}$$

where we introduced the tensor

$$L^{0\nu_1\nu_2}_{ijkl}(q) = \frac{2}{\beta N}\sum_{\boldsymbol{p},\omega_n}\tilde{G}^{\nu_1\nu_2}_{ij}(p+q)\tilde{G}^{\nu_2\nu_1}_{kl}(p). \tag{A3}$$

Following Ref. 20, we introduce a column vector $\mathcal{A}(=\mathcal{L},\mathcal{M})$ and a 4×4 matrix $\mathcal{D}$ as

$$\mathcal{A} = \begin{pmatrix}A_{11}\\A_{12}\\A_{21}\\A_{22}\end{pmatrix} \equiv \begin{pmatrix}A_1\\A_2\\A_3\\A_4\end{pmatrix}, \tag{A4}$$

$$\hat{\mathcal{D}} = \begin{pmatrix} L^0_{1111} & L^0_{1121} & L^0_{1211} & L^0_{1221} \\ L^0_{1112} & L^0_{1122} & L^0_{1212} & L^0_{1222} \\ L^0_{2111} & L^0_{2121} & L^0_{2211} & L^0_{2221} \\ L^0_{2112} & L^0_{2122} & L^0_{2212} & L^0_{2222}\end{pmatrix}. \tag{A5}$$

The GRPA equations are cast into the form

$$\bar{\mathcal{A}}^{\nu_1\nu_2}(q) = \mathcal{A}^{0\nu_1\nu_2}(q) + U\sum_{\nu_3}\hat{\mathcal{D}}^{\nu_1\nu_3}(q)\bar{\mathcal{A}}^{\nu_3\nu_2}(q), \tag{A6}$$

$$\mathcal{A}^{\nu_1\nu_2}(q) = \bar{\mathcal{A}}^{\nu_1\nu_2}(q) - U\sum_{\nu_3}\bar{\mathcal{L}}^{\nu_1\nu_3}(q)A^{\nu_3\nu_2}(q). \tag{A7}$$

The above equations are easily solved to give

$$\begin{pmatrix}A^{aa}(q) & A^{ab}(q)\\ A^{ba}(q) & A^{bb}(q)\end{pmatrix} = \begin{pmatrix}1+U\bar{L}^{aa}(q) & U\bar{L}^{ab}(q)\\ U\bar{L}^{ba}(q) & 1+U\bar{L}^{bb}(q)\end{pmatrix}^{-1} \times \begin{pmatrix}\bar{A}^{aa}(q) & \bar{A}^{ab}(q)\\ \bar{A}^{ba}(q) & \bar{A}^{bb}(q)\end{pmatrix}, \tag{A8}$$

$$\begin{pmatrix}\bar{\mathcal{A}}^{aa}(q) & \bar{\mathcal{A}}^{ab}(q)\\ \bar{\mathcal{A}}^{ba}(q) & \bar{\mathcal{A}}^{bb}(q)\end{pmatrix} = \begin{pmatrix}\hat{I}-U\hat{\mathcal{D}}^{aa}(q) & -U\hat{\mathcal{D}}^{ab}(q)\\ -U\hat{\mathcal{D}}^{ba}(q) & \hat{I}-U\hat{\mathcal{D}}^{bb}(q)\end{pmatrix}^{-1} \times \begin{pmatrix}\mathcal{A}^{0aa}(q) & \mathcal{A}^{0ab}(q)\\ \mathcal{A}^{0ba}(q) & \mathcal{A}^{0bb}(q)\end{pmatrix}. \tag{A9}$$

Here, we denoted $A^{\nu_1\nu_2} = \mathrm{Tr}\{\hat{A}^{\nu_1\nu_2}\} = \mathcal{A}_1^{\nu_1\nu_2} + \mathcal{A}_4^{\nu_1\nu_2}$.

APPENDIX B: ENERGY DISPERSION OF THE HIGGS MODE

We derive the analytic expression of the energy dispersion of the Higgs mode for small momentum $q \ll 1$ following the approach of Ref. 3. The gap equation (4) can be rewritten as

$$1 - \frac{U}{2N}\sum_{\boldsymbol{p}}\left(\frac{1}{E}+\frac{1}{E'}\right) = 0. \tag{B1}$$

We denote $E(\boldsymbol{p}) = E$, $E(\boldsymbol{p}+\boldsymbol{q}) = E'$, $\gamma = \gamma_{\boldsymbol{p}}$, and $\gamma' = \gamma_{\boldsymbol{p}+\boldsymbol{q}}$. Subtracting Eq. (B1) from $1 + U[(C+D) - |R|] = 0$, which is equivalent to Eq. (11), we obtain

$$U\,(X - |R|) = 0, \tag{B2}$$

where

$$X = (C+D) + \frac{1}{2N}\sum_{\boldsymbol{p}} \frac{E+E'}{EE'}$$
$$= \frac{1}{2N}\sum_{\boldsymbol{p}} \frac{E+E'}{EE'} \frac{\omega^2 - (|\gamma|^2 + |\gamma'|^2) - 4\Delta^2}{\omega^2 - (E+E')^2}. \tag{B3}$$

Here, we have replaced $i\Omega_n \to \omega$. At $\boldsymbol{q} = 0$, Eq. (B2) reduces to

$$\frac{y}{N}\sum_{\boldsymbol{p}} \frac{1}{E}\frac{1}{\omega^2 - 4E^2}$$
$$= y\int_0^{3t} d\varepsilon\, \frac{\rho(\varepsilon)}{\sqrt{\varepsilon^2+\Delta^2}[\omega^2 - 4(\varepsilon^2+\Delta^2)]} = 0, \tag{B4}$$

where $y = \omega^2/4 - \Delta^2$ and $\rho(\varepsilon) = \frac{1}{N}\sum_{\boldsymbol{p}} \delta(\varepsilon - |\gamma_{\boldsymbol{p}}|)$ is the density of states of the fermion energy band. If we set $\omega = 2\Delta$, the denominator in the integrand of Eq. (B4) is proportional to ε^2, while the numerator is proportional to ε for small ε because $\rho(\varepsilon) \propto \varepsilon$. The integral in Eq. (B4) is thus well defined in the limit $\omega \to 2\Delta$. In this limit, Eq. (B4) is satisfied when $y = 0$ and consequently the energy of the Higgs mode is obtained as $\omega_{\text{Higgs}}(\boldsymbol{q} = 0) = 2\Delta$.

To derive the energy dispersion for small $\boldsymbol{q}$, we expand Eq. (B2) to second order in $\boldsymbol{q}$. Using the relations

$$\gamma_{\boldsymbol{p}+\boldsymbol{q}} \simeq \gamma_{\boldsymbol{p}} + \delta\gamma_1 + \delta\gamma_2,\ \delta\gamma_1$$
$$= -it\{e^{i\boldsymbol{p}\cdot\boldsymbol{a}_1}(\boldsymbol{q}\cdot\boldsymbol{a}_1) + e^{i\boldsymbol{p}\cdot\boldsymbol{a}_2}(\boldsymbol{q}\cdot\boldsymbol{a}_2)\}, \tag{B5}$$

$$\delta\gamma_2 = \frac{t}{2}\{e^{i\boldsymbol{p}\cdot\boldsymbol{a}_1}(\boldsymbol{q}\cdot\boldsymbol{a}_1)^2 + e^{i\boldsymbol{p}\cdot\boldsymbol{a}_2}(\boldsymbol{q}\cdot\boldsymbol{a}_2)^2\}, \tag{B6}$$

$$w_1 = \text{Re}[\gamma^*\delta\gamma_1]$$
$$= -t^2\{[\sin(\boldsymbol{p}\cdot\boldsymbol{a}_1) + \sin(\boldsymbol{p}\cdot\boldsymbol{a}_3)](\boldsymbol{q}\cdot\boldsymbol{a}_1)$$
$$+ [\sin(\boldsymbol{p}\cdot\boldsymbol{a}_2) - \sin(\boldsymbol{p}\cdot\boldsymbol{a}_3)](\boldsymbol{q}\cdot\boldsymbol{a}_2)\}, \tag{B7}$$

$$w_1' = \text{Im}[\gamma^*\delta\gamma_1]$$
$$= t^2\{[1 + \cos(\boldsymbol{p}\cdot\boldsymbol{a}_1) + \cos(\boldsymbol{p}\cdot\boldsymbol{a}_3)](\boldsymbol{q}\cdot\boldsymbol{a}_1)$$
$$+ [1 + \cos(\boldsymbol{p}\cdot\boldsymbol{a}_2) + \cos(\boldsymbol{p}\cdot\boldsymbol{a}_3)](\boldsymbol{q}\cdot\boldsymbol{a}_2)\}, \tag{B8}$$

$$w_2 = \text{Re}[\gamma^*\delta\gamma_2]$$
$$= -\frac{t^2}{2}\{[1 + \cos(\boldsymbol{p}\cdot\boldsymbol{a}_1) + \cos(\boldsymbol{p}\cdot\boldsymbol{a}_3)](\boldsymbol{q}\cdot\boldsymbol{a}_1)^2$$
$$+ [1 + \cos(\boldsymbol{p}\cdot\boldsymbol{a}_2) + \cos(\boldsymbol{p}\cdot\boldsymbol{a}_3)](\boldsymbol{q}\cdot\boldsymbol{a}_2)^2\}, \tag{B9}$$

$$w_2' = \text{Im}[\gamma^*\delta\gamma_2]$$
$$= -\frac{t^2}{2}\{[\sin(\boldsymbol{p}\cdot\boldsymbol{a}_1) + \sin(\boldsymbol{p}\cdot\boldsymbol{a}_3)](\boldsymbol{q}\cdot\boldsymbol{a}_1)^2$$
$$+ [\sin(\boldsymbol{p}\cdot\boldsymbol{a}_2) - \sin(\boldsymbol{p}\cdot\boldsymbol{a}_3)](\boldsymbol{q}\cdot\boldsymbol{a}_2)^2\}, \tag{B10}$$

$$|\gamma_{\boldsymbol{p}+\boldsymbol{q}}|^2 \simeq |\gamma_{\boldsymbol{p}}|^2 + s_1 + s_2,\ s_1 = 2w_1,\ s_2 = |\delta\gamma_1|^2 + 2w_2, \tag{B11}$$

$$|\delta\gamma_1|^2 = t^2\{(\boldsymbol{q}\cdot\boldsymbol{a}_1)^2 + 2\cos(\boldsymbol{p}\cdot\boldsymbol{a}_3)(\boldsymbol{q}\cdot\boldsymbol{a}_1)(\boldsymbol{q}\cdot\boldsymbol{a}_2)$$
$$+ (\boldsymbol{q}\cdot\boldsymbol{a}_2)^2\}, \tag{B12}$$

one finds that Eq. (B3) becomes

$$X \simeq \frac{1}{2N}\sum_{\boldsymbol{p}} \frac{2}{E}\frac{\omega^2 - (2|\gamma|^2 + s_1 + s_2) - 4\Delta^2}{\omega^2 - 4E^2}$$
$$= \frac{1}{N}\sum_{\boldsymbol{p}} \frac{1}{E}\frac{\omega^2 - (2|\gamma|^2 + s_2) - 4\Delta^2}{\omega^2 - 4E^2}. \tag{B13}$$

Since the factor $\sin(\boldsymbol{p}\cdot\boldsymbol{a}_i)$ is odd for $\boldsymbol{p}$, the summation for $\boldsymbol{p}$ including this factor vanishes. Similarly, R can be approximated as

$$R \simeq -\frac{1}{N}\sum_{\boldsymbol{p}} \frac{2}{E}\frac{(\gamma + \delta\gamma_1 + \delta\gamma_2)\gamma^*}{\omega^2 - 4E^2}, \tag{B14}$$

$$\text{Re}R = -\frac{1}{N}\sum_{\boldsymbol{p}} \frac{2}{E}\frac{|\gamma|^2 + w_2}{\omega^2 - 4E^2} = R_0 + R_2, \tag{B15}$$

$$\text{Im}R = -\frac{1}{N}\sum_{\boldsymbol{p}} \frac{2}{E}\frac{w_1'}{\omega^2 - 4E^2} = R_1. \tag{B16}$$

In evaluating further Eqs. (B13), (B15), and (B16), we encounter the factor

$$\sum_{\boldsymbol{p}} \frac{1}{E}\frac{\cos(\boldsymbol{p}\cdot\boldsymbol{a}_i)}{\omega^2 - 4E^2}. \tag{B17}$$

Here, we replace $\cos(\boldsymbol{p}\cdot\boldsymbol{a}_i)$ in the integrand with its value at the K (K') point, i.e., $\langle\cos(\boldsymbol{p}\cdot\boldsymbol{a}_i)\rangle = \cos(\boldsymbol{p}_K\cdot\boldsymbol{a}_i) = -\frac{1}{2}$. At half-filling, since the Fermi level is at the K (K') point, this replacement is justified for small q. As a result, R_1 and R_2 vanish and we finally obtain

$$X - |R| \simeq \left(4y - v_F^2 q^2\right)\frac{1}{N}\sum_{\boldsymbol{p}} \frac{1}{E}\frac{1}{\omega^2 - 4E^2} = 0, \tag{B18}$$

where $v_F = 3t/2$ is the Fermi velocity. Consequently, the dispersion of the Higgs mode is obtained as

$$\omega_{\text{Higgs}}^2 = 4\Delta^2 + v_F^2 q^2. \tag{B19}$$

In the limit $\Delta^2 \gg v_F^2 q^2$, ω_{Higgs} is approximated as $\omega_{\text{Higgs}} = 2\Delta + v_F^2 q^2/4\Delta$, which is plotted in Fig. 1(f). On the other hand, at the transition point with $\Delta = 0$, the dispersion for small q coincides with that of the lower edge of the continuum as $\omega_{\text{Higgs}} = v_F q$.

1. Energy dispersion of the AB/Leggett mode

We derive the energy dispersion of the AB/Leggett mode for small momentum. Subtracting Eq. (B1) from $1 + U[(C - D) - \sqrt{4F^2 + |R|^2}] = 0$, which is equivalent to Eq. (11), we obtain

$$U(Y - \sqrt{4F^2 + |R|^2}) = 0, \tag{B20}$$

where

$$Y = (C-D) + \frac{1}{2N}\sum_{\boldsymbol{p}} \frac{E+E'}{EE'}$$
$$= \frac{1}{2N}\sum_{\boldsymbol{p}} \frac{E+E'}{EE'} \frac{\omega^2 - (|\gamma|^2 + |\gamma'|^2)}{\omega^2 - (E+E')^2}. \tag{B21}$$

Setting $\boldsymbol{q} = 0$, we obtain

$$Y = \frac{1}{N}\sum_{\boldsymbol{p}} \frac{1}{E}\frac{\omega^2 - 2|\gamma|^2}{\omega^2 - 4E^2} = d_1\omega^2 - 2d_2, \tag{B22}$$

$$R = -\frac{2}{N}\sum_{\boldsymbol{p}} \frac{1}{E}\frac{|\gamma|^2}{\omega^2 - 4E^2} = -2d_2, \tag{B23}$$

$$F = \frac{1}{N}\sum_{\boldsymbol{p}} \frac{1}{E}\frac{\Delta\omega}{\omega^2 - 4E^2} = d_2\Delta\omega, \tag{B24}$$

where

$$d_1(\omega) = \frac{1}{N}\sum_{\boldsymbol{p}} \frac{1}{E}\frac{1}{\omega^2 - 4E^2}, \tag{B25}$$

$$d_2(\omega) = \frac{1}{N}\sum_{\boldsymbol{p}} \frac{1}{E}\frac{|\gamma|^2}{\omega^2 - E^2}. \tag{B26}$$

Thus, Eq. (B20) reduces to

$$Y - \sqrt{4F^2 + |R|^2} = \frac{d_1\omega^2(d_1\omega^2 - 4d_2 - 4d_1\Delta^2)}{(d_1\omega^2 - 2d_2) + \sqrt{4d_1^2\Delta^2\omega^2 + 4d_2^2}} = 0. \tag{B27}$$

From $d_{i=1,2}(\omega < 2\Delta) < 0$, we obtain the gapless AB/Leggett mode: $\omega_{\mathrm{AB}}(\boldsymbol{q} = 0) = 0$. Note that the term within parentheses in the numerator of Eq. (B27) at $\omega = 0$ is found to give

$$-4d_2(\omega = 0) - 4d_1(\omega = 0)\Delta^2 = \frac{1}{N}\sum_{\boldsymbol{p}} \frac{1}{E} = \frac{1}{U}. \tag{B28}$$

For small $\boldsymbol{q}$, expanding F, R, and Y to second order in $\boldsymbol{q}$, we obtain

$$Y \simeq d_1\omega^2 - 2d_2 - d_1 v_F^2 q^2, \tag{B29}$$

$$F \simeq \Delta d_1\omega, \quad R \simeq -2d_2. \tag{B30}$$

In Eqs. (B29) and (B30), we used the same approximation as the one for Eq. (B18). As a result, we obtain

$$Y - \sqrt{4F^2 + |R|^2} \simeq \frac{d_1(\omega = 0)\left[\omega^2/U + 4d_2(\omega = 0)v_F^2 q^2\right]}{\left(d_1\omega^2 - 2d_2 - 2d_1 v_F^2 q^2\right) + \sqrt{4\Delta^2 d_1^2\omega^2 + 4d_2^2}} = 0. \tag{B31}$$

We have used Eq. (B28) to derive the final expression. The pole is thus given by

$$\omega_{\mathrm{AB}} = \lambda v_F q, \tag{B32}$$

$$\lambda^2 = 4U|d_2(\omega = 0)| = \frac{U}{N}\sum_{\boldsymbol{p}} \frac{|\gamma|^2}{E^3}. \tag{B33}$$

Note that $\lambda \leqslant 1$ from the gap equation (2). At the transition point ($\Delta = 0$), $\lambda = 1$ and thus the AB/Leggett mode becomes degenerate with the Higgs mode as well as the edge of the continuum as $\omega_{\mathrm{AB}} = v_F q$.

[1] C. M. Varma, J. Low Temp. Phys. **126**, 902 (2002).
[2] R. Sooryakumar and M. V. Klein, Phys. Rev. Lett. **45**, 660 (1980).
[3] P. B. Littlewood and C. M. Varma, Phys. Rev. Lett. **47**, 811 (1981); Phys. Rev. B **26**, 4883 (1982).
[4] See G. E. Volovik and M. A. Zubkov, Phys. Rev. D **87**, 075016 (2013) and references therein.
[5] K. Penc, J. Romhanyi, T. Room, U. Nagel, A. Antal, T. Feher, A. Janossy, H. Engelkamp, H. Murakawa, Y. Tokura, D. Szaller, S. Bordacs, and I. Kezsmarki, Phys. Rev. Lett. **108**, 257203 (2012).
[6] C. Rüegg, B. Normand, M. Matsumoto, A. Furrer, D. F. McMorrow, K. W. Krämer, H.-U. Güdel, S. N. Gvasaliya, H. Mutka, and M. Boehm, Phys. Rev. Lett. **100**, 205701 (2008).
[7] S. D. Huber, B. Theiler, E. Altman, and G. Blatter, Phys. Rev. Lett. **100**, 050404 (2008).
[8] U. Bissbort, S. Götze, Y. Li, J. Heinze, J. S. Krauser, M. Weinberg, C. Becker, K. Sengstock, and W. Hofstetter, Phys. Rev. Lett. **106**, 205303 (2011).
[9] M. Endres, T. Fukuhara, D. Pekker, M. Cheneau, P. Schauss, C. Gross, E. Demler, S. Kuhr, and I. Bloch, Nature (London) **487**, 454 (2012).
[10] L. Pollet and N. Prokof'ev, Phys. Rev. Lett. **109**, 010401 (2012).
[11] L. Tarruell, D. Greif, T. Uehlinger, G. Jotzu, and T. Esslinger, Nature (London) **483**, 302 (2012).
[12] I. Bloch, J. Dalibard, and W. Zwerger, Rev. Mod. Phys. **80**, 885 (2008).
[13] E. Zhao and A. Paramekanti, Phys. Rev. Lett. **97**, 230404 (2006).
[14] S. Tsuchiya, R. Ganesh, and A. Paramekanti, Phys. Rev. A **86**, 033604 (2012).
[15] S. Sorella, Y. Otsuka, and S. Yunoki, Sci. Rep. **2**, 992 (2012).
[16] Reference 15 has used quantum Monte Carlo simulations to establish the phase diagram of the *repulsive* Hubbard model with $t' = 0$. However, this model can be mapped onto the *attractive* model using a sublattice-dependent particle-hole transformation. See, e.g., S.-C. Zhang, Phys. Rev. Lett. **65**, 120 (1990).
[17] F. F. Assaad and I. Herbut, arXiv:1304.6340.
[18] P. Noziéres and F. Pistolesi, Eur. Phys. J. B **10**, 649 (1999).
[19] G. Baskaran and S. A. Jafari, Phys. Rev. Lett. **89**, 016402 (2002).
[20] R. Côté and A. Griffin, Phys. Rev. B **48**, 10404 (1993).
[21] See Appendix A.
[22] P. W. Anderson, Phys. Rev. **112**, 1900 (1958).
[23] Y. Nambu, Phys. Rev. **117**, 648 (1958).
[24] A. J. Leggett, Prog. Theor. Phys. **36**, 901 (1966).
[25] See Appendix B for the detailed derivation of the asymptotic dispersions of the AB/Leggett mode and the Higgs mode.
[26] Y. Nambu and G. Jona-Lasinio, Phys. Rev. **122**, 345 (1961).
[27] T. M. Rice, K.-Y. Yang, and F. C. Zhang, Rep. Prog. Phys. **75**, 016502 (2012).
[28] N. M. R. Peres, M. A. N. Araújo, and A. H. Castro Neto, Phys. Rev. Lett. **92**, 199701 (2004).

[29]M. E. Zhitomirsky and A. L. Chernyshev, Rev. Mod. Phys. **85**, 219 (2013).
[30]G. D. Mahan, *Many Particle Physics*, 2nd ed. (Plenum Press, New York, 1993).
[31]L. Pitaevskii and S. Stringari, *Bose-Einstein Condensation* (Oxford University Press, Oxford, 2003).
[32]Y. Barlas and C. M. Varma, Phys. Rev. B **87**, 054503 (2013).
[33]S. Gazit, D. Podolsky, and A. Auerbach, Phys. Rev. Lett. **110**, 140401 (2013).
[34]J. Ibañez-Azpiroz, A. Eiguren, A. Bergara, G. Pettini, and M. Modugno, Phys. Rev. A **87**, 011602(R) (2013).